Enhanced second-harmonic generation in media with a weak periodicity

J. W. Haus, R. Viswanathan, M. Scalora,* A. G. Kalocsai,† J. D. Cole,† and J. Theimer‡
Department of Physics, Rensselaer Polytechnic Institute, Troy, New York 12180-3590
(Received 4 February 1997)

First-order multiple-scale perturbation theory is used to derive a set of coupled-mode equations valid for electromagnetic-wave propagation in a weakly periodic, nonlinear medium with periodicity on the order of a wavelength. We apply this to a problem where the medium has a $\chi^{(2)}$ response and find that the second-harmonic signal generated is enhanced when the fundamental is tuned near the band edge. Results are given for a possible experiment with optical fibers. [S1050-2947(98)03703-2]

PACS number(s): 42.65.−k, 42.65.An

I. INTRODUCTION

Wave propagation in periodic dielectric materials is useful for developing a number of photonic devices [1], such as distributed feedback lasers [2] and Bragg grating filters [3]. The transmission is characterized by large dispersion of the pulse and the appearance of stop bands when the Bragg conditions are met. Recently, especially large group velocity delays have been reported at the edge of the stop band where the transmission is near unity and at the same time, the pulse experiences no appreciable change in its shape [4].

This paper is devoted to an analysis of second-harmonic frequency conversion in weakly periodic media with material periodicity chosen to be on the order of the fundamental harmonic wavelength. The tools of our analysis are multiple scale perturbation theory [5] and we carry out the calculations to demonstrate the potential for using a band edge resonance in Bragg gratings. A second paper deals with the numerical computations for deep gratings [6], but some of the qualitative understanding gleaned from the present analysis carries over to the analysis of deep gratings. Phase matching multiwave interactions by periodic structures was perhaps first discussed some time ago by Armstrong *et al.* [7] and by Bloembergen and Sievers [8].

Three types of phase matching were proposed by Armstrong *et al.* [7] for efficient harmonic generation. Among them, it was proposed to periodically replace the nonlinear medium by its inversion image every coherence length, which is proportional to the reciprocal of the phase mismatch wave number. This is called quasi-phase-matching; the nonlinear susceptibility changes sign, but the linear properties of the medium are the same. Generally, the coherence length is orders of magnitude longer than the fundamental wavelength. Theoretically, quasi-phase-matching preceded birefringent phase matching, but it was not experimentally feasible until recently, when periodic poling of the domains in a ferroelectric crystal was developed [9]. Other concepts similar to phase matching were also proposed [10]. For quasi-phase-matching to be efficient, the length scale of the material periodicity is on the order of the coherence length; for this length scale periodically varying the nonlinear coefficient is important.

However, there are some signaling problems where the material periodicity is on the order of a wavelength. Here the linear properties of the medium become important and can be used to reduce the phase mismatch arising from nonlinear wave mixing. In this regime, because of the chosen periodicity, only the spatial dc component of the (possibly) periodically varying nonlinear coefficient is required. We dub this band-edge phase matching; it is distinct from other forms of phase matching, such as using a defect mode in the periodic structure [11,12]. Band-edge phase matching is so chosen because the fundamental wavelength is near the band edge of the first stop band in the structure and forward-backward wave coupling is resonant. Band-edge phase matching can be considered the converse of quasi-phase-matching in terms of which medium properties are homogeneous or periodic. In quasi-phase-matching the linear medium appears homogeneous and the nonlinear medium is periodic with the period chosen to be of the order of the coherence length. However, in band-edge phase matching the linear medium is periodic and the nonlinear medium appears homogeneous with the periodicity on the order of a wavelength.

As an application of a second-harmonic medium for the processes discussed in this paper, we propose the use of silica glass fibers. Despite the disorder in glass, second-harmonic generation was observed, first in fibers [13,14], then in bulk glasses [15], as well. Conversion efficiency approaches several percent.

A fiber Bragg grating is an example of a weakly periodic medium. They have a number of applications; filters, taps, and wavelength division multiplexers are a few examples, but others have been demonstrated, such as laser wavelength control, mode conversion in fibers, and distributed Bragg reflectors [3]. Furthermore, chirped fiber Bragg gratings have been used to compress pulses broadened by self-phase modulation. For instance, pulses have been compressed from 2 ps duration to less than 200 fs duration [16].

Nonlinear optical mixing effects in fibers can incorporate Bragg gratings to improve the optical conversion of radiation. The design features require good overlap of the optical

*Permanent address: U.S. Army Missile Command, Weapons Sciences Directorate, AMSMI-RD-WS-ST Redstone Arsenal, AL 35898-5248.

†Permanent address: Department of Mathematical Sciences, Rensselaer Polytechnic Institute, Troy, NY 12180-3590.

‡Permanent address: Rome Laboratory, RL/OCPA, 25 Electronics Parkway, Rome, NY 13441-4515.

energy in the fiber grating; advantages are a reduced, grating-dependent group velocity to increase the interaction time of the waves in the grating, matching of the phase velocities, and band-edge resonance to increase the mode amplitude in the structure. The design of periodic structures will lead to higher conversion efficiency, more compact structures, and lower input power requirements. Enhancement of conversion efficiency in deep gratings has been numerically examined [6], but so far no complete analysis of the problem has been made, nor has the problem been examined in fibers. This paper is intended to place the previous findings on a firm mathematical footing; in this we are partially successful by analyzing the case of weakly periodic gratings with periodicity on the order of a wavelength.

In applying multiple scales to the time dependent pulse problem, we assume the medium to have chromatic dispersion even at the lowest perturbative order. This is slightly different from the usual Kronig-Penney model, where chromatic dispersion is neglected [1]. Time-dependent secularity conditions are different for chromatic dispersive and nondispersive problems and must be handled separately. However, for the time-independent cw problem, multiple scales can handle both the chromatic dispersive and nondispersive cases at once, because secularity conditions reduce to those of spatial harmonic Fourier terms, provided the physical problem can be reduced to a finite set of spatial oscillators. We derive evolution equations for the chromatic dispersion case; and for the continuous wave problem, we derive results with chromatic dispersion and then show how the parameters reduce to the dispersionless case to illustrate what is obtained in Kronig-Penney-type models. Note that for band-edge phase matching to occur, chromatic dispersion is required in order to be offset by the Bragg grating dispersion, as will be shown by first-order perturbation theory.

II. COUPLED-MODE EQUATIONS

We consider a wave incident upon a nonlinear medium. The medium has a periodic modulation of the dielectric constant; for the one-dimensional case the form of Maxwell's equation is

$$\frac{\partial^2 E}{\partial z^2}-\frac{1}{c^2}\frac{\partial^2 D_L}{\partial t^2}=\frac{4\pi}{c^2}\frac{\partial^2 P^{\mathrm{NL}}}{\partial t^2}. \tag{1}$$

D_L is the linear displacement field, which is related to the electric field by the following constitutive relation:

$$D_L(z,t)=\int_{-\infty}^{t}\epsilon(z,t-t')E(z,t')dt'. \tag{2}$$

The function $\epsilon(z,t)$ is the dielectric function; it is periodic in z and the medium is dispersive. P^{NL} is the nonlinear polarization contribution, which for our present case is a second-order nonlinearity.

$$P^{\mathrm{NL}}=\lambda\chi^{(2)}E^2. \tag{3}$$

Here λ is a parameter that multiplies a perturbative contribution; there are five smaller parameters in our analysis and this parameter serves as a bookkeeping device. In this context λ is a dimensionless parameter that will be set to one after the perturbation analysis is carried out; it serves to identify all the contributions of a given perturbative order.

The coefficient $\chi^{(2)}$ governs three-wave-mixing processes, e.g., sum- and difference-frequency and second-harmonic generation. The analysis given hereafter can also be applied to a number of three-wave-mixing processes, but we restrict our attention to second-harmonic generation. The analysis can also be extended to include four-wave mixing by introducing a third-order susceptibility.

Before deriving the coupled-mode equations, Eq. (2) is rewritten by introducing the Fourier transform relation

$$\epsilon(z,t)=\int\hat{\epsilon}(z,\omega)e^{-i\omega t}d\omega. \tag{4}$$

The function $\hat{\epsilon}(z,\omega)$ is complex and its real and imaginary parts are denoted by the subscripts r and i, respectively. By using the Taylor-series expansion of $\hat{\epsilon}(z,\omega)$, Eq. (2) can be expressed in a local form:

$$D_L(z,t)=\hat{\epsilon}\left(z,i\frac{\partial}{\partial t}\right)E(z,t). \tag{5}$$

This expression is well suited to the multiple-scale analysis given below. The real part of the dielectric function is of order unity, but the imaginary part is considered to be weak, i.e., $\hat{\epsilon}(\omega)=\hat{\epsilon}_r(\omega)+i\lambda\hat{\epsilon}_i(\omega)$. The function $\hat{\epsilon}$ is a periodic function in z. For a weakly periodic medium we assume the form

$$\hat{\epsilon}(z,\omega)=\hat{\epsilon}(\omega)+\lambda 2\Delta\hat{\epsilon}(\omega)\cos(2\pi z/d). \tag{6}$$

Here d is the period of the dielectric variation and $\Delta\hat{\epsilon}(\omega)$ is the amplitude of the spatially periodic component.

A. Multiple-scale analysis

In the multiple-scale analysis [5] the space and time coordinates are expanded in a power series of a small parameter that we denote as λ; $t_n=\lambda^n t_0$ and $z_n=\lambda^n z_0$. In the past this method has been applied to $\chi^{(2)}$ materials without periodic changes by two of the authors [17]; the procedure parallels that development, except that, here, we truncate the expansion at first-order perturbation theory. The spatial and temporal derivatives are

$$\begin{aligned}\frac{\partial}{\partial t}&=\frac{\partial}{\partial t_0}+\lambda\frac{\partial}{\partial t_1}+\cdots,\\ \frac{\partial}{\partial z}&=\frac{\partial}{\partial z_0}+\lambda\frac{\partial}{\partial z_1}+\cdots.\end{aligned} \tag{7}$$

Similarly, the electric field is also expanded in powers of the perturbation parameter

$$E=E_0+\lambda E_1+\cdots. \tag{8}$$

Orders of the perturbation parameter λ are gathered together. Besides the spatial variations of the dielectric function, the nonlinearity and absorption are also considered to be weak, as noted above by the parameter λ. The expansion of the real part of the dielectric function to first order is

$$\hat{\epsilon}_r\left(i\frac{\partial}{\partial t}\right)=\hat{\epsilon}_r\left(i\frac{\partial}{\partial t_0}\right)+\lambda\hat{\epsilon}_r'\left(i\frac{\partial}{\partial t_0}\right)i\frac{\partial}{\partial t_1}. \tag{9}$$

The prime denotes a derivative with respect to the argument of the function, i.e., frequency. The $O(1)$ term in the expansion is

$$L_0E_0=\left[\frac{\partial}{\partial z_0^2}-\frac{1}{c^2}\frac{\partial^2}{\partial t_0^2}\hat{\epsilon}_r\left(i\frac{\partial}{\partial t_0}\right)\right]E_0=0. \tag{10}$$

The solution, when a plane wave is incident at $z=0$ with a frequency ω and 2ω, is expressed as

$$\begin{aligned}E_0=&\frac{A_{f1}(z_1,t_1)}{\sqrt{k_1}}e^{i(k_1z_0-\omega t_0)}+\frac{A_{b1}(z_1,t_1)}{\sqrt{k_1}}e^{i(-k_1z_0-\omega t_0)}\\&+\frac{A_{f2}(z_1,t_1)}{\sqrt{k_2/2}}e^{i(k_2z_0-2\omega t_0)}+\frac{A_{b2}(z_1,t_1)}{\sqrt{k_2/2}}e^{i(-k_2z_0-2\omega t_0)}\\&+\text{c.c.},\end{aligned} \tag{11}$$

where the wave numbers (k_1,k_2) are obtained from the chromatic dispersion properties of a bulk homogeneous medium, so that $k_1^2=\omega^2\hat{\epsilon}_r(\omega)/c^2$ and $k_2^2=(2\omega)^2\hat{\epsilon}_r(2\omega)/c^2$. In our analysis the phase mismatch is also treated as small, i.e., $\lambda\Delta k=(k_2-2k_1)$. Note that $\lambda\Delta kz_0=\Delta kz_1$. Hence at the first-order perturbation, the traditional three-wave process is obtained where quadratic nonlinearities dominate. We avoid large phase mismatch because that would lead to an asymptotic regime beyond three-wave mixing (or cascading) [17]. The field amplitudes depend on the slower parameters (z_1,t_1) and the rapid variations of the field appear as a plane wave solution of the wave equation. The amplitudes of the fundamental waves (A_{f1},A_{b1}) and the second-harmonic waves (A_{f2},A_{b2}) are treated as order unity functions, which multiply the plane-wave solutions.

To first order in λ the equations of motion are

$$\begin{aligned}L_0E_1=&\frac{1}{c^2}\left[\frac{\partial^2}{\partial t_0^2}i\hat{\epsilon}_i\left(i\frac{\partial}{\partial t_0}\right)E_0\right]-2\left[\frac{\partial^2}{\partial z_0\partial z_1}E_0\right.\\&\left.-\frac{1}{c^2}\frac{\partial^2}{\partial t_1\partial t_0}\hat{\epsilon}_r\left(i\frac{\partial}{\partial t_0}\right)E_0\right]+\frac{1}{c^2}\frac{\partial^2}{\partial t_0^2}\hat{\epsilon}_r'\left(i\frac{\partial}{\partial t_0}\right)i\frac{\partial E_0}{\partial t_1}\\&+\frac{2\cos(2\pi z_0/d)}{c^2}\frac{\partial^2}{\partial t_0^2}\Delta\hat{\epsilon}_r\left(i\frac{\partial}{\partial t_0}\right)E_0\\&+\frac{4\pi\chi^{(2)}}{c^2}\frac{\partial^2}{\partial t_0^2}E_0^2.\end{aligned} \tag{12}$$

The chromatic dispersive secular terms are eliminated from the right hand side of Eq. (12), as shown in Refs. [5,17]. We also choose the grating periodicity d so that it is close to one-half of the fundamental harmonic wavelength. The deviation from this condition is denoted by $2\lambda\delta=2\pi/d-2k_1$ and from that we observe $2\lambda\delta z_0=2\delta z_1$. At the fundamental frequency, forward-backward waves are coupled because of the choice of grating periodicity d. The equations of motion for the fundamental frequency envelope functions are given by

$$\begin{aligned}\frac{\partial A_{f1}}{\partial z_1}+\frac{1}{v_{g1}}\frac{\partial A_{f1}}{\partial t_1}=&-\frac{\pi}{d}\frac{\alpha_1}{2}A_{f1}+i\frac{\pi}{d}\kappa A_{b1}e^{i2\delta z_1}\\&+i\frac{\pi}{d}NA_{f2}A_{f1}^*e^{i\Delta kz_1},\\-\frac{\partial A_{b1}}{\partial z_1}+\frac{1}{v_{g1}}\frac{\partial A_{b1}}{\partial t_1}=&-\frac{\pi}{d}\frac{\alpha_1}{2}A_{b1}+i\frac{\pi}{d}\kappa A_{f1}e^{-i2\delta z_1}\\&+i\frac{\pi}{d}NA_{b2}A_{b1}^*e^{-i\Delta kz_1}.\end{aligned} \tag{13}$$

The group velocity at the fundamental frequency is $v_{g1}=d\omega/dk_1$; at this first-order perturbation level, the group velocity on the left hand side is that of the homogeneous medium, because of the corresponding wave number k_1 that was defined earlier. The expansion procedure of multiple scales does not allow anything else [17]. The normalized absorption coefficient is $\alpha_1=(d/\pi)(\omega_0^2/k_1c^2)\hat{\epsilon}_i(\omega_0)$ and the normalized grating strength coefficient is $\kappa=(d/\pi)\Delta\hat{\epsilon}\omega_0^2/(2k_1c^2)$. The scaled nonlinear coefficient is $N=(d/\pi)\omega_0^2 4\pi\chi^{(2)}/(k_1c^2\sqrt{k_2/2})$.

The second-harmonic equations are given by

$$\begin{aligned}\frac{\partial A_{f2}}{\partial z_1}+\frac{1}{v_{g2}}\frac{\partial A_{f2}}{\partial t_1}=&-\frac{\pi}{d}\frac{\alpha_2}{2}A_{f2}+i\frac{\pi}{d}NA_{f1}^2e^{-i\Delta kz_1},\\-\frac{\partial A_{b2}}{\partial z_1}+\frac{1}{v_{g2}}\frac{\partial A_{b2}}{\partial t_1}=&-\frac{\pi}{d}\frac{\alpha_2}{2}A_{b2}+i\frac{\pi}{d}NA_{b1}^2e^{i\Delta kz_1},\end{aligned} \tag{14}$$

where the group velocity at the second harmonic is $v_{g2}=d(2\omega)/dk_2$, where again, at first-order perturbation theory, this is the group velocity of the homogeneous medium and the normalized absorption coefficient is $\alpha_2=(d/\pi)(4\omega_0^2/k_2c^2)\hat{\epsilon}_i(2\omega_0)$. The forward and backward waves at the second harmonic are not coupled in the weak-grating limit, unless a second sinusoidal variation of the dielectric function is added so that $2\pi l/d-2k_2\sim O(\lambda)$, where l is an integer.

To simplify the equations we scale the length: $z_1\rightarrow(\pi/d)z_1$ and the field amplitudes are scaled to the nonlinear coefficient, so that $a_{f1}=NA_{f1}e^{-i\pi\delta_1z_1/d}$, $a_{b1}=NA_{b1}e^{i\pi\delta_1z_1/d}$, $a_{f2}=NA_{f2}e^{i\pi\delta_2z_1/d}$, and $a_{b2}=NA_{b2}e^{-i\pi\delta_2z_1/d}$. Here $\delta_1=(d/\pi)\delta$ and $\delta_2=(d/\pi)\Delta k-2\delta_1$. The scaled form of the equations of motion for the fundamental fields are

$$\begin{aligned}\frac{\partial a_{f1}}{\partial z_1}+\frac{d}{\pi v_{g1}}\frac{\partial a_{f1}}{\partial t_1}=&-\frac{\alpha_1}{2}a_{f1}-i\delta_1a_{f1}+i\kappa a_{b1}+ia_{f2}a_{f1}^*,\\-\frac{\partial a_{b1}}{\partial z_1}+\frac{d}{\pi v_{g1}}\frac{\partial a_{b1}}{\partial t_1}=&-\frac{\alpha_1}{2}a_{b1}-i\delta_1a_{b1}+i\kappa a_{f1}\\&+ia_{b2}a_{b1}^*.\end{aligned} \tag{15}$$

The scaled equations for the second harmonic become

$$\frac{\partial a_{f2}}{\partial z_1}+\frac{d}{\pi v_{g2}}\frac{\partial a_{f2}}{\partial t_1}=-\frac{\alpha_2}{2}a_{f2}+i\delta_2a_{f2}+ia_{f1}^2, \tag{16}$$

$$-\frac{\partial a_{b2}}{\partial z_1}+\frac{d}{\pi v_{g2}}\frac{\partial a_{b2}}{\partial t_1}=-\frac{\alpha_2}{2}a_{b2}+i\delta_2 a_{b2}+ia_{b1}^2.$$

The above equations were derived for pulses in strongly chromatic dispersive media. For the cw envelope, it does not matter whether the medium is chromatic or achromatic, because the spatial-dependent equations remain the same (except that $\Delta k=0$ for achromatic media). However, for pulses in weakly dispersive or achromatic materials, the evolution equations are quite different and the above equations do not apply. The above equations were derived under the assumption that grating dispersion is used to compensate chromatic dispersion.

B. Band-edge phase matching

The weak grating differs from the homogeneous medium through the addition of two parameters (δ_1,κ), as shown in Eqs. (15) and (16). Harmonic enhancement is obtained by careful choices of these parameters, and based on the dispersion properties of the material. Note that in this model chromatic dispersion dominates grating dispersion and the results obtained here are different from the usual Kronig-Penney models [1], which neglects chromatic dispersion.

It must be mentioned that the parameters (δ_1,δ_2) can be related to the frequency detuning $\omega-\omega_0=\lambda\Delta$. Here $\omega_0=\pi c/dn(\omega_0)$, which is the scaled frequency for the center of the first stop band. From the previous definitions of (δ_1,k_1) we find

$$\frac{d}{\pi}k_1(\omega)=1-\lambda\delta_1=\frac{d}{\pi}\frac{\omega}{c}n(\omega). \tag{17}$$

Expanding in a Taylor series about ω_0 we obtain

$$\frac{d}{\pi}k_1(\omega_0)=1+\lambda\Delta\left[\frac{1}{\omega_0}+\frac{n'(\omega_0)}{n(\omega_0)}\right]. \tag{18}$$

The prime denotes a derivative with respect to angular frequency. Therefore, the scaled deviation parameter δ_1 becomes

$$\delta_1=-\Delta\left[\frac{1}{\omega_0}+\frac{n'(\omega_0)}{n(\omega_0)}\right]. \tag{19}$$

For a material with no chromatic dispersion, i.e., $n(\omega)=$const, only the first term is relevant in Eq. (19) and

$$\frac{d}{\pi}k_1(\omega_0)=1+\frac{\lambda\Delta}{\omega_0}. \tag{20}$$

This is expected in the Kronig-Penney-type models.

From Eq. (19), δ_1 is proportional to the frequency detuning Δ multiplied by a function of ω_0. The parameter δ_2 is the difference between the phase mismatch Δk and $2\delta_1$ and is given as

$$\delta_2=\frac{d}{\pi}\Delta k-2\delta_1. \tag{21}$$

The band-edge phase matching is obtained by choosing $\delta_2=0$. We choose δ_1 to offset the phase mismatch Δk due to chromatic dispersion. This implies the alternate condition

$$n(2\omega)-n(\omega)=\frac{\pi c\delta_1}{\omega d}. \tag{22}$$

At ω_0 this is approximately

$$n(2\omega_0)-n(\omega_0)+\lambda\Delta[2n'(2\omega_0)-n'(\omega_0)]=\frac{\pi c\delta_1}{d(\omega_0+\lambda\Delta)}. \tag{23}$$

If the dispersion is such that $2n'(2\omega_0)-n'(\omega_0)\sim O(\lambda)$, then it may be neglected. We define $\Omega=\omega_0+\lambda\Delta$. Under these approximations the band-edge phase matching condition becomes

$$n(2\omega_0)-n(\omega_0)=\frac{\pi c\delta_1}{d\Omega}. \tag{24}$$

There are two cases when the band-edge phase matching condition cannot be obtained. These occur when $\Delta k=0$ or $\delta_1=0$, independently. The first case denotes the material is chromatically nondispersive; from Eqs. (19) and (21), we see that $\delta_2=-2\delta_1=2\Delta/\omega_0$. Here we have a Kronig-Penney-type model with only a Bragg grating and there is no chromatic dispersion to offset. The second case shows that $\delta_2=d\Delta k/\pi$. Here the material is chromatic, but the detuning from the band gap center frequency is zero because of Eq. (19). Here the transmission is attenuated and the second-harmonic generation is not efficient.

To get the most out of band-edge phase matching, we have to utilize the two independent grating parameters (δ_1,κ). The best value for δ_1 may be inferred without solving Eqs. (15) and (16), but adjusting κ requires the examination of solutions. By imposing the condition $\delta_2=0$, the chromatic dispersion can be compensated by the dispersion of the Bragg grating, i.e., adjusting δ_1. At the band edge the phases introduced by forward and backward wave coupling change the phases of the waves in the material and this condition no longer assures the best conversion efficiency, as will be illustrated below. κ can be adjusted by changing the modulation depth $\Delta\hat{\epsilon}$, so that the best phase matching is concurrently coincident with a transmission resonance of the grating. The transmission resonances, discussed below, are further evidence of strong forward-backward wave coupling and this leads to a an enhancement of the second-harmonic field.

C. Steady-state, nondepleted solutions

The equations can be solved for the nondepleted pump and steady-state fields. This case illustrates the essential desirable features of the grating that enhance the nonlinear response of the material. Absorption is also neglected.

The steady-state equations for the fundamental field amplitude are

$$\frac{\partial a_{f1}}{\partial z_1}=-i\delta_1 a_{f1}+i\kappa a_{b1}, \tag{25}$$

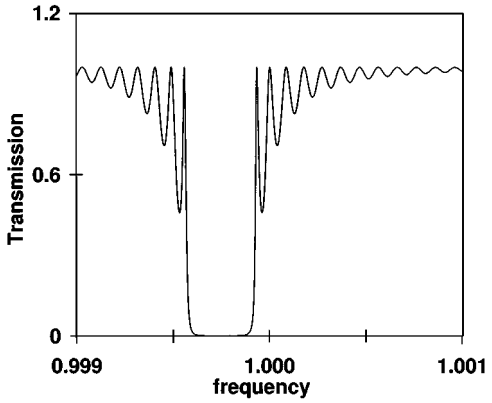

FIG. 1. Transmission vs frequency for a 10^4 period grating (or in scaled units $L=\pi 10^4$) with a dielectric variation of $\Delta\hat{\epsilon}=5\times10^{-4}$. The mode-coupled results and the transfer matrix calculations are indistinguishable.

$$\frac{\partial a_{b1}}{\partial z_1}=i\delta_1 a_{b1}-i\kappa a_{f1}. \tag{26}$$

Defining $\Delta_1=\sqrt{\delta_1^2-\kappa^2}$, which is the effective wave number for the envelope on the z_1 scale, one can obtain the corresponding grating group velocity (for the infinite medium)

$$V_G=\Delta_1/\delta_1. \tag{27}$$

This is not the same as the group velocities appearing on the left hand side of Eqs. (15) and (16), but a correction to the homogeneous medium group velocity in second-order perturbation theory, which is not developed here but done in [17] for other effective wave numbers for the envelope. The solutions to the above equations are

$$a_{f1}(z)=\left(\cos(\Delta_1 z_1)-\frac{i\delta_1}{\Delta_1}\sin(\Delta_1 z_1)\right)a_{f1}(0)+\frac{i\kappa}{\Delta_1}\sin(\Delta_1 z_1)a_{b1}(0), \tag{28}$$

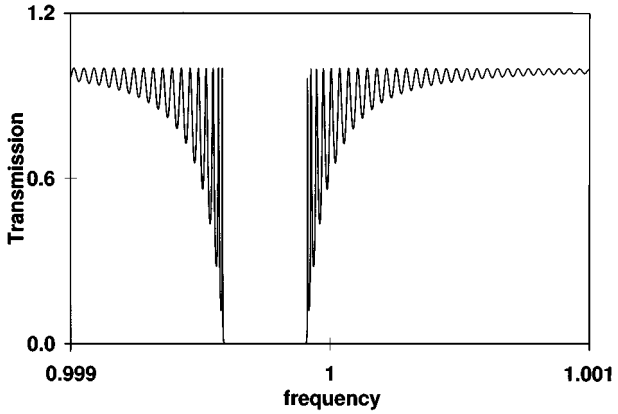

FIG. 2. Transmission vs frequency for a structure with 2.5×10^4 periods, i.e., $L=2.5\pi\times10^4$. See Fig. 1 for parameters.

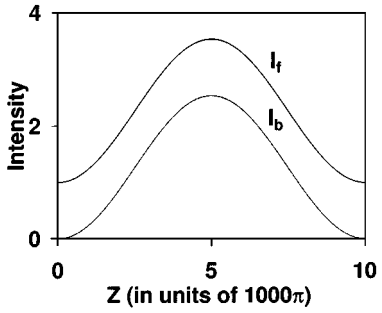

FIG. 3. The forward- and backward-propagating field intensities, when the detuning is set at the first transmission maximum on the lower band edge, as a function of position (z in units of $\pi10^3$). For parameter details see Fig. 1.

$$a_{b1}(z)=\left(\cos(\Delta_1 z_1)+\frac{i\delta_1}{\Delta_1}\sin(\Delta_1 z_1)\right)a_{b1}(0)-\frac{i\kappa}{\Delta_1}\sin(\Delta_1 z_1)a_{f1}(0). \tag{29}$$

We consider a medium with N periods; in scaled units the sample length is $L=\pi N$. The input field $a_{f1}(0)$ is normalized to 1, and applying the boundary condition that the backward field vanishes at L, gives the reflected field amplitude

$$a_{b1}(0)=\frac{i\kappa\,\sin(\Delta_1 L)}{\Delta_1\,\cos(\Delta_1 L)+i\delta_1\,\sin(\Delta_1 L)}. \tag{30}$$

The transmittance through the structure is simply $T=|a_{f1}(L)|^2$.

The results are illustrated by considering the following index variation $\Delta\hat{\epsilon}=5\times10^{-4}$, with $\epsilon_1=1$ and $\epsilon_2=1+2\Delta\hat{\epsilon}$. The average dielectric constant is 1.0005. Figures 1 and 2 are plots of the transmission $|a_{f1}(L)|^2/|a_{f1}(0)|^2$ versus frequency for $L=\pi10^4$ and $L=2.5\pi\times10^4$, respectively. The analytically calculated curves are indistinguishable from those generated by a transfer matrix routine with a step index profile whose first Fourier coefficient is identical to $\Delta\hat{\epsilon}$. We note that the center of the gap is displaced from unity because the average refractive index is not unity.

The transmission oscillations at the band edges are called transmission resonances. They have a close correspondence

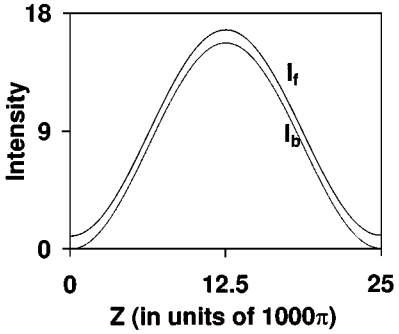

FIG. 4. The forward- and backward-propagating field intensities, when the detuning is set at the first transmission maximum on the lower band edge, as a function of position (z in units of $\pi10^3$). The chosen parameters correspond to Fig. 2.

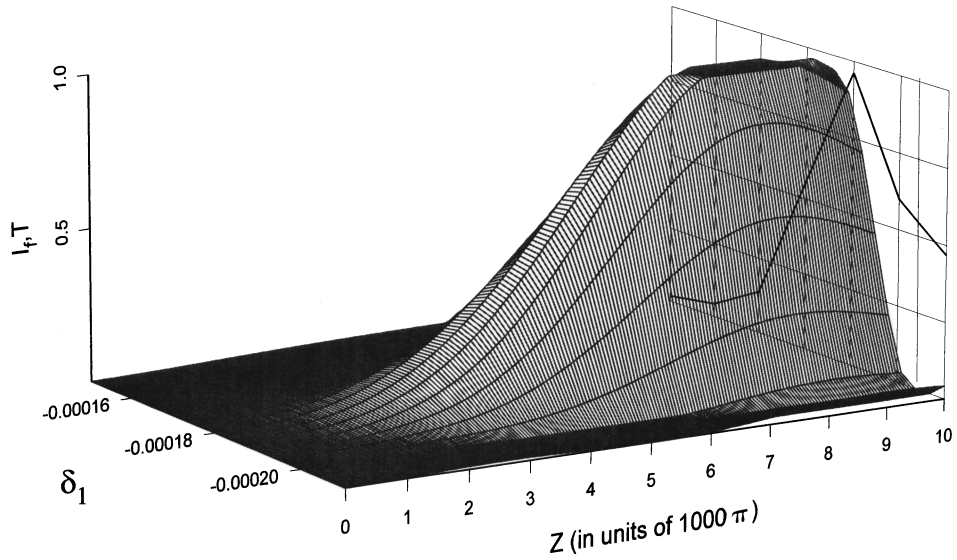

FIG. 5. Forward-propagating second-harmonic intensity in the medium vs position and phase matching frequency for a 10^4 period structure. The vertical axis has been scaled by 8. The side panel shows the transmission spectrum for the fundamental wave.

with Fabry-Pérot-like resonances of the envelope functions in the structure. The field amplitudes corresponding to the first transmission resonances at the lower edge of the stop band are plotted in Figs. 3 and 4; these display the change of the amplitude by increasing the number of periods. As would be found for the lowest transmission resonance in a Fabry-Pérot etalon, the field amplitude has one maximum. The difference here is that the Fabry-Pérot resonance is half a wavelength, while for the Bragg grating, field amplitude is slowly varying over the scale of the wavelength. The input field is normalized to unity. The forward- and backward-propagating amplitudes have a single extremum and their maxima exceed the input field value. The maximum value increases as the number of periods, N, increases. The maximum field amplitude is proportional to $\Delta\hat{\epsilon}$ and increases with this parameter as well. For large dielectric contrast between the layers only a few layers suffice to enhance the field beyond its input value [6]. This can be used to design compact frequency conversion structures.

The second-harmonic fields are simply solved by applying the Laplace transform technique to Eq. (16); in general, the solutions are complicated and we do not present them here. In the following sections we will analyze the solutions in detail.

III. RESULTS

The second-harmonic fields at the transmission maximum are enhanced by the transmission resonance of the fundamental field. In homogeneous media the fields are phase

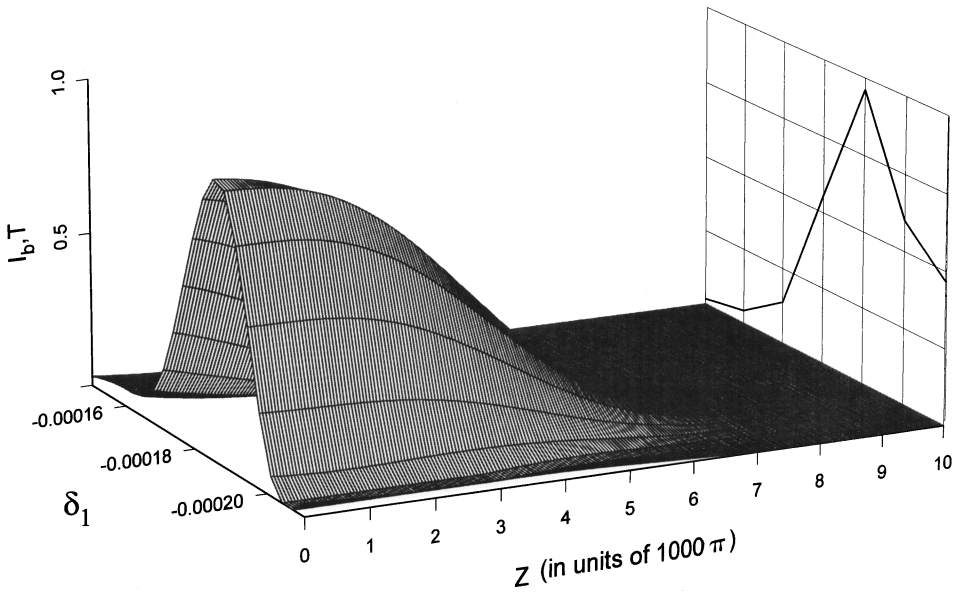

FIG. 6. Backward-propagating second-harmonic intensity in the medium vs position and phase matching frequency for a 10^4 period structure. The vertical axis has been scaled by 8. The side panel shows the transmission spectrum for the fundamental wave.

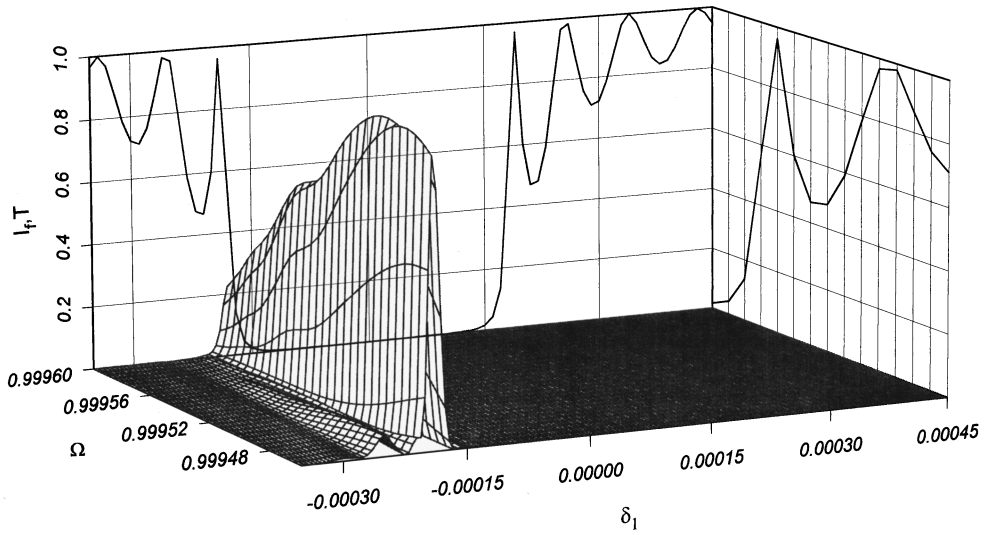

FIG. 7. The plot of the forward-propagating second-harmonic intensity in the medium vs phase matching and detuning for a 2.5×10^4 period structure. The vertical axis has been scaled by 16. The side panels show the transmission spectrum for the fundamental wave.

matched, i.e., $\Delta k=0$, to assure that the best conversion efficiency is achieved. However, as mentioned above, the optimal condition for conversion is not identical to the phase matching condition without the backward propagating fields which are coupled by the grating period and lead to the parameter $2\delta_1$ compensating for Δk. The interplay of forward and backward fields gives additional position-dependent phase shifts to the complex amplitudes.

Figures 5 and 6 display the behavior of the second-harmonic fields in the medium as a function of frequency, but assuming $\delta_2=0$ at each frequency, i.e., Ω is the frequency of the fundamental field. The forward, second-harmonic field in Fig. 5 is zero at the input, but increases at the output, a maximum increase occurs when the phase matching frequency corresponds to the maximum of the transmission curve, which is also drawn on the side panel.

The output second-harmonic intensity has been scaled to the second harmonic generated from a perfectly phase matched homogeneous medium of the same length and nonlinear response. The enhancement of the forward-propagating output at the maximum is about 16 times that of the homogeneous case. The second harmonic is roughly proportional to the square of the intensity, so the large second harmonic can be mainly attributed to the enhanced first-harmonic field at the transmission resonance, which is nearly a factor of 4. For a 2.5×10^4 period grating, the enhancement is about 400 times above the homogeneous medium, when the fields are phase matched. Note we remain within the nondepleted pump approximation and the second harmonic is still weak compared to the fundamental.

The second-harmonic backward wave is also enhanced by about a factor of 4 above the homogeneous medium. Again by reference to Fig. 3 this is consistent with the enhanced fundamental-harmonic backward field inside the medium. The forward and backward fields form a standing-wave pattern in the sample at the transmission resonance and although the fundamental field is absent in the reflection at the transmission peak, the backward second-harmonic has a maximum there. The backward-propagating second-harmonic intensity is a probe of the backward fundamental field in the medium, just as the forward-propagating second harmonic probes its fundamental field.

Finally, the sharpness of the response with phase matching is gauged from Figs. 7 and 8 for the forward- and backward-propagating second-harmonic fields, respectively. The fields have been scaled by a factor of 16 and the side panels display the transmission curves for the fundamental. The maximum for a given value of δ_1 occurs at the first transmission maximum; the output is sharply peaked at that frequency with a spectral width about as wide as the transmission resonance. This occurs for both the forward and the backward fields. The forward propagating, second-harmonic field is the strongest, since it has the largest field at the transmission resonance, as previously discussed. Since the fields are not phase matched at the upper transmission maximum, there is no perceptible output on this scale of intensities. Also, drawing attention to the side panel on the Ω axis, we note the maximum conversion does not occur when $\delta_2=0$ at the first transmission maximum; instead, the best conversion efficiency occurs for $\delta_2=0$ at the second transmission maximum. This is a consequence of the additional phase changes due to presence of both forward and backward fields in the medium. The weak secondary maxima observed in both figures is due to the resonance at the second transmission maximum. Including medium dispersion in the analysis is an important aspect of designing efficient conversion devices.

IV. CONCLUDING REMARKS

The fields are affected by several factors at the band edge. First, there is a Fabry-Pérot-type resonance in the field amplitudes, which leads to higher conversion efficiencies inside the structure. The field amplitude is large over a major portion of the volume. Second, the transmission is large, so that all the fundamental field will enter the structure, i.e., there is no impedance mismatch. Third, the grating group velocity at

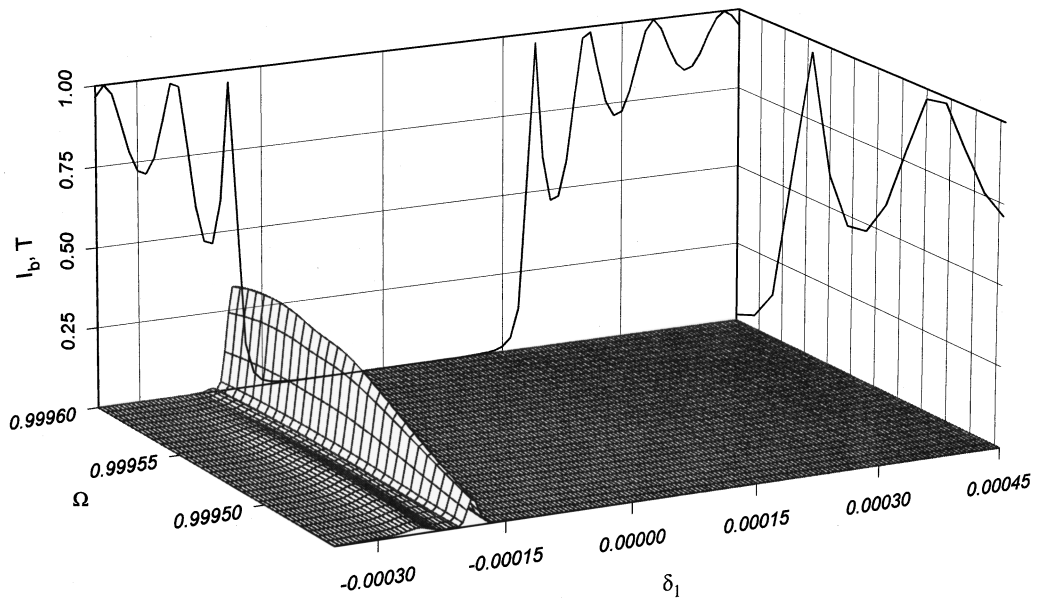

FIG. 8. Plot of the backward-propagating second-harmonic intensity in the medium vs phase matching and detuning for a 10^4 period structure. The vertical axis has been scaled by 16. The side panel shows the transmission spectrum for the fundamental wave.

the band edge is small and the fundamental field under appropriate conditions described by higher-order perturbation theory or deep gratings may spend more time inside the structure leading to greater conversion efficiency. In our model, the grating group velocity is dominated by that of homogeneous chromatic media. Our results are quite distinct from quasi-phase-matching, which involves a different length scale; the medium periodicity is chosen on the order of a coherence length and modulating the nonlinear coefficient is important. The contrast with band-edge phase matching is apparent; since the grating periodicity is on the order of a wavelength, the linear properties of the medium are utilized to reduce the phase mismatch, as described by the parameter δ_2.

There are design parameters whose determination is important for applications of this analysis. The phase matching condition is not easily defined here due to the interaction of the forward and backward waves; nevertheless, there are optimal values of δ_1 that provide enhanced conversion. The matching frequency and the transmission maxima should be tuned for the best results. This means that for a given amplitude, $\Delta\hat{\epsilon}$, there is an optimum number of layers that will achieve this condition. The number of layers should be large enough to result in an increased conversion efficiency; on the other hand, the maximum number of layers is set by technological limits, but the larger the number of periods, the sharper the transmission resonances in frequency space (compare Figs. 1 and 2). This sets a lower limit on the pulse duration, since if the pulse is too short, then its spectrum extends over several transmission maxima, which leads to pulse dispersion, reflection, and reshaping in the structure.

Second-harmonic fields have been generated in glass hosts, despite the fact that it is on the average centrosymmetric. This centrosymmetry can be broken by adding a static external field or by defects seeded in the medium during the three-wave-mixing process. Fiber Bragg gratings written into prepared fibers could be used to demonstrate the resonance enhancement concept. The conversion is already good for the prepared fiber and it could be further increased by writing a Bragg grating into the fiber. The index change in the core could be of order 0.01 [18] and the overlap of a mode with the core is typically around 75%, so that the efficiency of the coupling is not significantly reduced [19].

Finally, the results here apply to a number of nonlinear conversion phenomena. The sum- and difference-frequency generation problems are amenable to the analysis given here. The coupled-mode equations are similar, but now depend linearly on the fundamental field. Third-order processes can also be treated by the same approach; the third-harmonic generation process depends on the cube of the fundamental field and greater efficiency can be achieved by the band-edge resonance; there is an additional gap near the third-harmonic frequency that provides a further resonance condition. For wavelengths below about 400 nm though, absorption will have to be included in the analysis. Other nonlinear processes can also be optimally designed at the band-edge for instance, the stimulated Raman scattering could be suppressed by tuning the fundamental field to the upper band-edge resonance or the amplification of fields and quantum coherence between the Stokes and anti-Stokes fields [20] could be managed by band-edge changes in the electromagnetic density of states.

ACKNOWLEDGMENTS

This research was partially supported by NSF Grant Nos. DMS-9510728 and ECS-9630068, and J.W.H. was supported by Rome Laboratories through Grant No. F30602-96-2-0056.

[1] A. Yariv and P. Yeh, *Optical Waves in Crystals* (John Wiley and Sons, New York, 1984).
[2] H. Kogelnik and C. V. Shank, J. Appl. Phys. **43**, 2328 (1972); M. Nakamura, A. Yariv, H. W. Yen, S. Somekh, and H. L. Garvin, Appl. Phys. Lett. **22**, 515 (1973).
[3] K. O. Hill, B. Malo, F. Bilodeau, and D. C. Johnson, Annu. Rev. Mater. Sci. **23**, 125 (1993).
[4] M. Scalora, R. J. Flynn, S. B. Reinhardt, R. L. Fork, M. J. Bloemer, M. D. Tocci, C. M. Bowden, J. P. Dowling, and R. P. Leavitt, Phys. Rev. E **54**, R1078 (1996).
[5] J. Kevorkian and J. D. Cole, *Perturbation Methods in Applied Mathematics* (Springer-Verlag, New York, 1981).
[6] M. Scalora, A. S. Manka, M. J. Bloemer, J. P. Dowling, C. M. Bowden, R. Viswanathan, and J. W. Haus, Phys. Rev. A **56**, 3166 (1997).
[7] J. A. Armstrong, N. Bloembergen, J. Ducuing, and P. S. Pershan, Phys. Rev. **127**, 1918 (1962).
[8] N. Bloembergen and A. J. Sievers, Appl. Phys. Lett. **17**, 483 (1970).
[9] M. Yamada, N. Nada, M. Saitoh, and K. Watanabe, Appl. Phys. Lett. **62**, 435 (1993); W. K. Burns, W. McElhanon, and L. Goldberg, IEEE Photonics Technol. Lett. **6**, 252 (1994); M. M. Fejer, G. A. Magerl, D. H. Jundt, and R. L. Byers, IEEE J. Quantum Electron. **28**, 2631 (1992); Q. Chen and W. P. Risk, Electron. Lett. **30**, 1516 (1994).
[10] S. Somekh and A. Yariv, Appl. Phys. Lett. **21**, 140 (1972); Opt. Commun. **6**, 301 (1972).
[11] J. Martorell and R. Corbalan, Opt. Commun. **108**, 319 (1994).
[12] J. Trull, R. Vilaseca, J. Martorell, and R. Corbalan, Opt. Lett. **20**, 1746 (1995).
[13] Y. Sasaki and Y. Ohmori, Appl. Phys. Lett. **39**, 466 (1981).
[14] U. Osterberg and W. Margulis, Opt. Lett. **11**, 516 (1986).
[15] T. J. Driscoll and N. M. Lawandy, Opt. Lett. **19**, 7 (1994).
[16] J. A. R. Williams, I. Bennion, and L. Zhang, IEEE Photonics Technol. Lett. **7**, 491 (1995).
[17] A. G. Kalocsai and J. W. Haus, Phys. Rev. E **52**, 3166 (1995); Phys. Rev. A **49**, 574 (1994).
[18] P. Lamaire, R. M. Atkins, V. Mizrahi, and W. A. Reed, Electron. Lett. **29**, 1191 (1993).
[19] G. P. Agrawal, *Fiber-optic Communication Systems* (John Wiley and Sons, New York, 1992), pp. 37–39.
[20] K. C. Yeong, J. W. Haus, and A. Chizhov, Phys. Rev. A **53**, 3606 (1996).